JOURNAL OF MATERIALS SCIENCE 31 (1996) 5083–5092

# Alumina–mullite–zirconia composites

## Part 1 *Colloidal processing and phase-formation characteristics*

H. M. JANG, S. M. CHO, K. T. KIM*
*Department of Materials Science and Engineering and *Department of Mechanical Engineering, Pohang University of Science and Technology (POSTECH), Pohang 790–784, Republic of Korea*

A boehmite–silica–zirconia precursor powder with a uniform spatial distribution of constitutive phases was prepared from the corresponding ternary sol by compressing the electrical double layer (EDL) without altering the magnitude of the surface potential at a pH of 3.5. Both the rheological data and the calculated potential energy of interaction indicated that the mixed ternary sol formed weakly coagulated units in a shallow potential energy well after the compression of EDL at a pH of 3.5. The effects of $\alpha$-$Al_2O_3$ seeding on the phase-formation characteristics were then systematically examined. It was observed that the $\alpha$-$Al_2O_3$ seeding facilitated the formation of $\alpha$-$Al_2O_3$ but that it suppressed the growth of mullite in the alumina–mullite–zirconia composite. These observations were attributed to the epitaxial effect of $\alpha$-$Al_2O_3$ seeds which preferentially induced the formation of corundum phase over mullite formation.

## 1. Introduction

Extensive research effort has been expanded in order to improve the mechanical properties of $Al_2O_3$ based ceramics. Amongst these mechanical properties, toughening resulting from dispersed $ZrO_2$ particles is the single most extensively studied area [1–3]. When the $ZrO_2$ inclusions have tetragonal symmetry, the toughening and concomitant strengthening have been attributed to the volume and shape changes associated with the stress-induced tetragonal → monoclinic (t → m) transformation, which occurs in the stress field of propagating cracks [1–5]. On the other hand, the microcrack nucleation at transformed m-$ZrO_2$ particles in zirconia-toughened alumina (ZTA) occurs in the stress field of propagating cracks, leading to an increase in fracture toughness comparable to that achieved by the stress-induced t → m transformation [1, 3, 6, 7].

Unfortunately, at temperatures above 700 °C, most $ZrO_2$-toughened ceramics cannot be used for load-bearing engineering parts. It seems that the following three factors are mainly responsible for the observed degradation in the high-temperature mechanical properties of $ZrO_2$ dispersed composites: (i) an increase in the thermodynamic stability of the tetragonal phase and thus a decrease in the driving force for the t → m martensitic transformation [7, 8] ; (ii) a decrease in the residual (thermal, elastic) strain and thus a decrease in the driving force for the microcrack nucleation [7] and (iii) high creep rates caused by the presence of intergranular films [9].

In order to improve the high-temperature mechanical properties of $ZrO_2$ toughened ceramics, various strengthening strategies have been attempted [9]. Amongst these the prevention of glassy intergranular phases appears to be a highly promising approach. It has been proposed [9] that the degradation of the high-temperature mechanical properties of $ZrO_2$ toughened ceramics can be improved by the incorporation of mullite ($3Al_2O_3 \cdot 2SiO_2$). It has been discussed [9] that the intergranular phases in mullite–zirconia composites mainly exist at the grain junctions rather than at grain boundaries (non-wetting grain boundaries). Therefore, the degration of mechanical properties due to the presence of amorphous intergranular films can be overcome in mullite–zirconia composites. Furthermore, mullite itself has excellent high-temperature structural properties, especially high creep resistance up to ~1300 °C [10, 11].

In view of these facts, the incorporation of mullite into ZTA composites is expected to improve its high-temperature mechanical properties. Therefore, alumina–mullite–zirconia (abbreviated as AMZ hereafter) composites potentially have excellent mechanical properties over a wide range of temperatures. A few studies have been reported on AMZ composites [12–14]. However, to date the fabrication of AMZ composites, has been limited to the reaction sintering method using zircon and alumina as starting materials. Furthermore, due to problems associated with *in situ* chemical reaction, microstructural control of the composites was unsuccessful.

The present article proposes and tests a new colloidal processing scheme for fabricating a dense AMZ composite with a uniform microstructure. Ultrafine ( < 100 nm) boehmite, Ludox silica, and monoclinic

0022–2461  

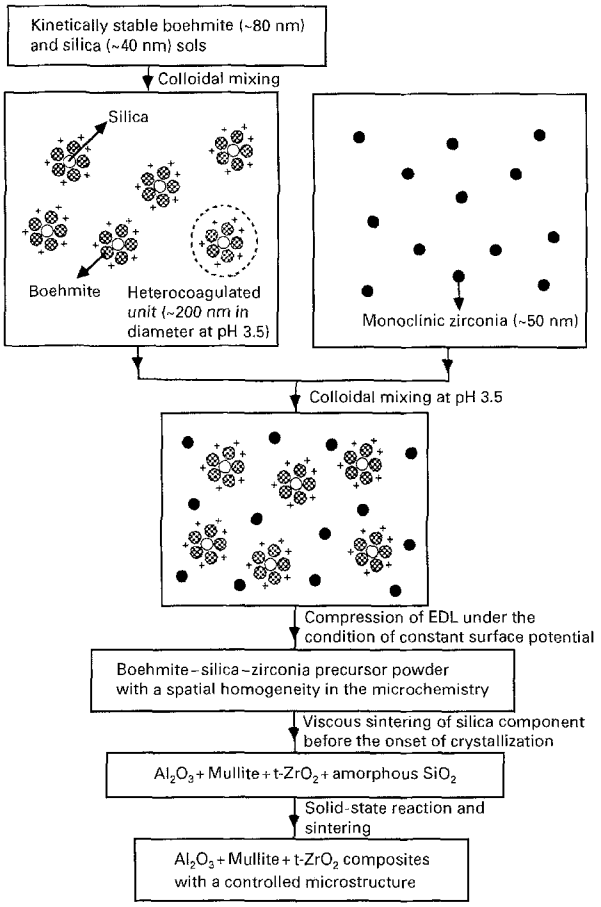


*Figure 1* Schematic diagram showing the basic concepts of the fabrication of alumina–mullite–zirconia composite by a colloidal processing route.

zirconia powders were used as the starting materials. It is reported that $\alpha$-$Al_2O_3$ seeding significantly lowers the transformation temperature of a boehmite gel and subsequently improves the microstructure of alumina [15, 16]. The effects of $\alpha$-$Al_2O_3$ seeding on the phase-formation characteristics and the densification behaviour of AMZ composites were also systematically examined. The basic concept of the fabrication of AMZ composites (or multicomponent ceramics, in general) used in this study is illustrated in Fig. 1. The present article focuses on the development of a colloidal processing scheme and also the phase-formation mechanisms of a boehmite–silica–zirconia precursor system. The microstructural development and the toughening of sintered AMZ composites are the subjects of a forthcoming paper [17].

## 2. Experimental procedure

A commercial Ludox $SiO_2$ powder (AS-40, Du Pont Chem. Co., USA) was used as the source of silica in the present study. It had an average size for the primary particle, determined by a transmission electron microscope (TEM), of 40 nm. The average particle size of the boehmite powder (Disperal Boehmite, Remet Chem. Co., Chadwicks, NY, USA) as determined by a laser-light scattering experiment was approximately 80 nm at pH 3.5, and its specific surface area was 160 $m^2 g^{-1}$. A pure, undoped monoclinic zirconia powder (UEP, Daichi Kigenso Kagaku Kogyo Co., Japan) was used as the source of zirconia. The average particle size in the zirconia sol at a pH of 3.5 was 50 nm. Unless otherwise specified, the composition of the AMZ composites used in this study is 50 wt% alumina–30 wt% mullite–20 wt% zirconia (after sintering).

The $\alpha$-$Al_2O_3$ seeds were prepared by a colloidal size separation of commercially available $\alpha$-$Al_2O_3$ (average particle size, 0.4 μm; AL-160SG-1, Showa Denko, Japan). The average particle size of the $\alpha$-$Al_2O_3$ seeds used in this study was 0.2 μm (200 nm), and more than 90% of the seed particles were within the range of 100–300 nm.

An electrokinetic stability of the colloidal suspension is an important factor for the homogeneous fabrication of a multicomponent precursor powder. The electrophoretic mobility of particles in a colloidal sol was determined by the electrophoretic laser-light scattering method (Zetasizer III, Malvern Instruments Co., Malvern, England). Detailed experimental descriptions of the sample preparation and the measurement of electrophoretic mobility were given in a previous article [18]. The zeta ($\zeta$) potential as a function of sol pH was estimated from the electrophoretic mobility data and the ionic conductivity (ionic strength) using the method of Wiersema, Loeb, and Overbeek [19].

Optimum conditions for the fabrication of a boehmite–silica–zirconia precursor powder from colloidal sols were deduced from rheological data. Rheological flow characteristics of colloidal sols were determined using a concentric cylinder viscometer (Model RV-100/CV-100, Haake, Germany). Steady rotational flow curves (i.e., shear stress versus shear rate) were generated by increasing the shear rate from zero to the maximum desired value, in 2 min, immediately followed by decreasing the shear rate back to zero in another 2 min. The amount of solid in the boehmite–silica–zirconia mixed sol is approximately 15 wt%.

In the fabrication of a boehmite–silica–zirconia precursor powder, a kinetically stable boehmite sol at pH 3.5 and a silica sol at pH 8 were first prepared separately using electrostatic stabilization. The desired amount of silica was incorporated into the boehmite sol by a slow dropwise addition of the silica sol under intense stirring whilst maintaining the pH at 3.5. The mixed sol was kinetically stable with a $\zeta$-potential of + 43 mV. The boehmite–silica binary sol was then mixed with the separately prepared zirconia sol while stirring at a pH of 3.5. The boehmite–silica–zirconia ternary sol at pH ~ 3.5 was apparently stable. In order to minimize any phase segregation amongst constituent sol particles, and thus, maintaining spatial homogeneity in the distribution of dispersed $ZrO_2$ particles in the resulting composite, ammonium carbonate solution was introduced under intense stirring. The pH of the ternary sol was maintained at a constant value by a simultaneous dropwise addition of nitric acid whilst the pH value was constantly monitored. The addition of salt to the mixed sol caused it to gel rapidly by the compression of the electrical double layer (EDL). This essentially eliminated the problems associated with differential settling and produced

a composite powder with a uniform distribution of constituent phases.

The wet gel was then dried in an oven at 100 °C. The dried gel was calcined at 500 °C for 4 h. The calcined powders were then pressed into pellets and cold-isostatically-pressed under a pressure of 2000 kg cm$^{-2}$. The compacts were then sintered in air at various temperatures below 1600 °C for 1 h with both heating and cooling rates of 5 °C per min. Sintered compacts were analysed for phase content using an X-ray diffractometer (DMAX-3B, Rigaku, Japan). Since stabilized cubic $ZrO_2$ was absent in the present composites, the relative phase fractions for the dispersed $ZrO_2$ polymorphs were determined with Cu $K_\alpha$ radiation using the method of Garvie and Nicholson [20].

## 3. Results and discussion

### 3.1. Colloidal processing of precursor powder

Fig. 2 shows the zeta potential data of silica, boehmite, zirconia, and the mixed sol containing boehmite and silica as a function of sol pH without adding any external electrolyte to control the ionic strength. The isoelectric points (IEP) of silica, boehmite, and zirconia are 2.7, 8.8 and 5.8, respectively. The zeta potential characteristics of boehmite are similar to those of $\alpha$-$Al_2O_3$ [21, 22]. The mixed sol consists of a mixture of boehmite and silica with the volume ratio of 7.7 : 1 and thus corresponds to 50 wt% alumina: 30 wt% mullite in the resulting composites after sintering. As shown in Fig. 2, its pH dependence of the zeta potential resembles that of boehmite rather than that of silica.

Laser-light scattering experiments indicated that the particle size of the boehmite–silica mixed sol at pH 3.5 was slightly less than 200 nm in diameter and increased rapidly above a pH of 4. As previously mentioned, the average diameter of silica and that of boehmite were 40 nm and 80 nm, respectively. The zeta potential of the mixed sol at pH 3.5 was + 43 mV (Fig. 2). From these experimental observations (particle size and zeta potential), one can conclude that a negatively charged silica particle is surrounded by several positively charged boehmite particles via electrostatic interaction, and this heterocoagulated aggregate, approximately 200 nm in diameter, forms a colloidal unit in the boehmite–silica mixed sol at a pH of 3.5. The mixed sol is also kinetically stable by virtue of its high zeta potential. Further evidence of the colloidal stability was obtained by examining rheological behaviour of the mixed sol at the pH of 3.5. As is shown in Fig. 3, the boehmite–silica binary sol at a pH of 3.5 is characterized by Newtonian behaviour. This suggests that there is no strong attractive interaction between the heterocoagulated units. The zeta potential data of the binary sol near pH 3.5 ( + 40–45 mV; Fig. 2) also support this conclusion.

Since the zirconia is also stable at a pH of 3.5 ( + 37 mV in $\zeta$-potential; Fig. 2), the two sols (i.e., the zirconia sol and the boehmite–silica binary sol) can be admixed uniformly whilst maintaining a good colloidal stability. The boehmite–silica–zirconia ternary sol was also apparently stable near a pH of 3.5. As is shown in Fig. 3, the rheological behaviour of the ternary sol is represented by nearly Newtonian flow. This indicates that the boehmite–silica–zirconia mixed sol does not form coagulated units in a deep potential

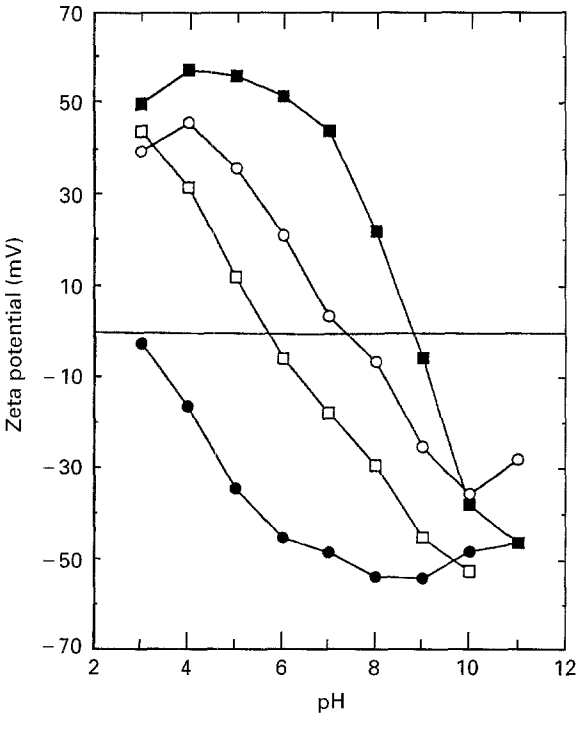


*Figure 2* Zeta potentials of; (■) boehmite, (●) silica, (□) zirconia and (○) boehmite–silica binary sols as a function of pH.

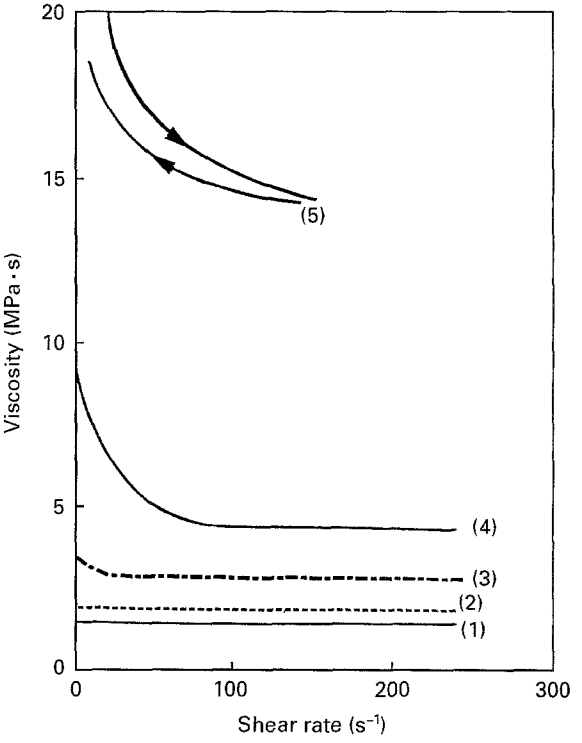


*Figure 3* Viscosity of various sols plotted as a function of shear rate. The systems studied are (1) boehmite–silica mixed sol at pH = 3.5, (2) zirconia sol at pH = 3.5, (3) boehmite–silica–zirconia ternary sol at pH = 3.5 before the compression of EDL, (4) boehmite–silica–zirconia ternary sol at pH = 3.5 after the compression of EDL and (5) boehmite–silica–zirconia ternary sol at pH = 7.

energy well (primary minimum). As a semi-quantitative approximation, the surface potential ($\psi_0$) of a ceramic (metal oxide) dispersion can be represented by the following Nernst-type equation [23]:

$$\psi_0 = \{2.303\, kT/e\} \cdot (\mathrm{pH}_0 - \mathrm{pH}) \quad (1)$$

where $\mathrm{pH}_0$ is the pH of the bulk medium at which the surface charge density becomes zero (point of zero charge (PZC) or IEP), $k$ is the Boltzmann constant, and $e$ is the unit electronic charge. The surface potentials estimated by the Nernst approximation are $\sim 310$ mV for the boehmite sol and $\sim 140$ mV for the zirconia sol at a pH of 3.5. These values of $\psi_0$ are large enough to prevent boehmite and zirconia particles from coagulating in the deep primary minimum in the interparticle potential energy.

Since $H^+$ and $OH^-$ are the two potential-determining ions (PDI) for metal oxides, the surface potential of a given aqueous sol is solely determined by the pH value, as discussed in Equation 1. Thus, the addition of an inert electrolyte other than $H^+$ and $OH^-$ to the above ternary sol would simply increase the ionic strength of the aqueous medium without significantly altering the magnitude of the surface potential ($\psi_0$) and cause it to gel rapidly by the compression of the electrical double layer (EDL). Since the surface potential essentially remains constant, the particles form weakly attractive units in a shallow potential-energy well (secondary minimum) rather than in the deep primary minimum [23, 24], thereby avoiding the formation of an irregular, randomly coagulated network.

Based on this idea, an inert electrolyte (ammonium carbonate solution) was added to the mixed ternary sol. Since the time scale involved in a given double-layer relaxation (i.e., the time needed by an ion to diffuse through the thickness of EDL) is very short [24], the increase of ionic strength immediately induces gelation or coagulation. This essentially eliminates the problems associated with the phase segregation (or differential settling) and eventually produces a composite precursor powder with a uniform spatial distribution of constitutive phases. This is the key idea of the present processing scheme.

As is shown in Fig. 3, the rheological flow curve of the ternary sol after the compression of EDL (at a pH of 3.5) is represented by pseudoplastic behaviour, and not by thixotropic behaviour. On the other hand, the increase of pH of the sol to 7 (near IEP of the mixed sol) then immediately induces a rapid coagulation in the primary potential-energy minimum (Smoluchowski limit). As expected, the ternary sol coagulated at the pH of 7 exhibits thixotropic behaviour (Fig. 3). Therefore, the viscosity data further support the previous conclusion that the compression of EDL at a pH of 3.5 without altering the surface potential leads to the formation of a weakly coagulated network in the shallow secondary potential-energy minimum.

A transmission electron micrograph of the boehmite–silica–zirconia composite powder calcined at 500 °C for 4 h is shown in Fig. 4. The darker particles are monoclinic $ZrO_2$. As is shown in Fig. 4, the size of

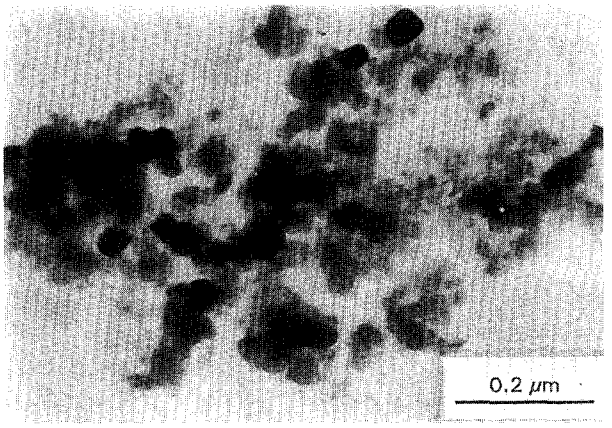


*Figure 4* Transmission electron micrograph of boehmite–silica–zirconia composite powder calcined at 500 °C for 4 h.

the primary $ZrO_2$ particles is approximately 50 nm (0.05 μm), and this value is exactly consistent with that of the $ZrO_2$ sol determined by the laser light-scattering method at a pH of 3.5. This clearly indicates that the zirconia sol was well-dispersed without any extensive coagulation at a pH of 3.5.

## 3.2. Potential energy of interaction

Our strategy on the colloidal processing of mixed precursor powder by the compression of EDL without altering the surface potential is further supported by examining the potential energy of interaction between approaching colloid particles. In our experimental conditions, the total interaction energy of two approaching particles ($V_{tot}$) is the sum of two contributions, which are the electrostatic repulsion due to an overlap of two diffuse electrical double layers ($V_R$) and the London-van der Waals attraction ($V_A$). Using the DLVO (Derjaguin–Landau–Verwelf–Overbeek) theory, the interaction energy of two dissimilar spherical particles with radii $a_1$ and $a_2$ in cgs units can be written as [25, 26]:

$$V_{tot}(S_0) = V_R + V_A \quad (2)$$

$$V_R = \frac{\varepsilon a_1 a_2 (\psi_{01}^2 + \psi_{02}^2)}{4(a_1 + a_2)} \left\{ \frac{2\psi_{01}\psi_{02}}{(\psi_{01}^2 + \psi_{02}^2)} \ln \frac{[1 + \exp(-\kappa S_0)]}{[1 - \exp(-\kappa S_0)]} + \ln[1 - \exp(-2\kappa S_0)] \right\} \quad (3)$$

$$\kappa = (8\pi n e^2 z^2 / \varepsilon k T)^{1/2} \quad (4)$$

$$V_A = -\frac{A}{12}\left\{ \frac{v}{u^2 + uv + u} + \frac{v}{u^2 + uv + u + v} + 2\ln\frac{u^2 + uv + u}{u^2 + uv + u + v} \right\} \quad (5)$$

$$u = S_0/2a_2 \quad \text{and} \quad v = a_1/a_2 \quad \text{for} \quad a_1 > a_2 \quad (6)$$

where $\varepsilon$ is the relative dielectric permittivity of the medium (78.5 for aqueous dispersion), $1/\kappa$ is the Debye–Hückel length, $S_0$ is the surface-to-surface distance of separation between two approaching particles, $n$ is the bulk concentration of electrolyte ions

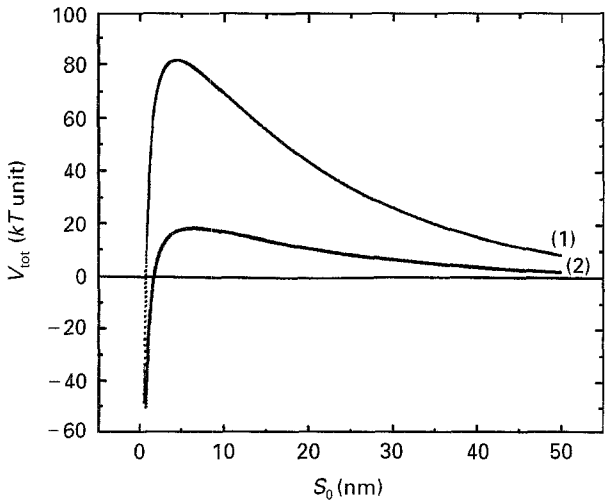


*Figure 5* Potential energy of homointeraction ($V_{tot}$) for (1) boehmite–silica sol ($a_1 = a_2 = 100$ nm) and (2) zirconia sol ($a_1 = a_2 = 25$ nm) as a function of the surface-to-surface distance of separation for a $\Psi_0$ of + 40 mV.

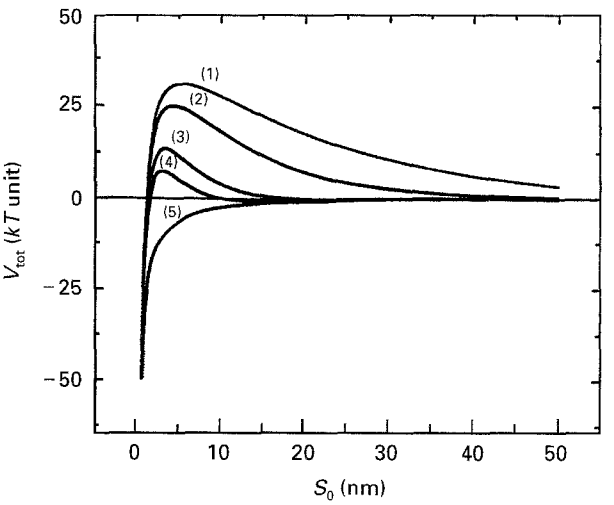


*Figure 6* Potential energy of heterointeraction between boehmite–silica composite particle ($a_1 = 100$ nm) and zirconia particle ($a_2 = 25$ nm) for a $\Psi_0$ of + 40 mV under the conditions of ionic strength of; (1) $\kappa = 5.85 \times 10^5$ cm$^{-1}$ ($10^{-3.5}$ M), (2) $\kappa = 1.04 \times 10^6$ cm$^{-1}$ ($10^{-3}$ M), (3) $\kappa = 2.33 \times 10^6$ cm$^{-1}$ ($5 \times 10^{-3}$ M), (4) $\kappa = 3.29 \times 10^6$ cm$^{-1}$ ($10^{-2}$ M) and (5) $\kappa = 1.04 \times 10^7$ cm$^{-1}$ ($10^{-1}$ M).

present in the medium, and $z$ is the valence of counter-electrolytes. $\psi_0$ in Equation 3 is the surface (coulombic) potential which can be replaced, to a good approximation, by the zeta potential under the condition of thermal Brownian collision [24]. Equation 3 is valid for the condition of constant low surface potential. $A$ in Equation 5 is the Hamaker constant and depends on the physical properties of particles and dispersion medium. The Hamaker constant of the aqueous boehmite sol was approximated by that of the aqueous alumina sol. The Hamaker constants used in the present calculation were taken from the work of Bleier and Westmoreland [27]. These are $4.5 \times 10^{-20}$ J, $1.39 \times 10^{-19}$ J, and $7.9 \times 10^{-20}$ J for boehmite, zirconia, and boehmite–zirconia aqueous sols, respectively.

Fig. 5 shows the calculated potential energy of homointeraction ($V_{tot}$) for the boehmite–silica sol ($a_1 = a_2 = 100$ nm) and that for zirconia sol ($a_1 = a_2 = 25$ nm) as a function of the surface-to-surface distance of separation for $\psi_{01} = \psi_{02} \approx \zeta = +$ 40 mV at a pH of 3.5. Since the volume ratio of boehmite/silica is 7.7: 1 and the boehmite–silica mixed sol forms heterocoagulated colloidal units, the Hamaker constant of the binary sol was simply replaced by that of boehmite sol. This does not affect our conclusion on the stability of the boehmite–silica mixed binary sol. The calculated potential energy of interaction indicates that the boehmite–silica sol at a pH of 3.5 ($\zeta = +$ 40 mV) is characterized by a large value of the potential energy barrier ($\sim 80\ kT$). Contrary to this, the zirconia sol is represented by a significantly smaller potential energy barrier ($\sim 20\ kT$) and seems to be close to the stability boundary. However, as discussed previously, both the viscosity data (Fig. 3) and the TEM result (Fig. 4) clearly indicate that the zirconia sol at a pH of 3.5 is kinetically stable with the absence of rapid Brownian coagulation. Since the zeta potential is the lower limit of the surface potential, the calculated potential energy barrier shown in Fig. 5 ($\sim 20\ kT$) also corresponds to the lower limit value. Therefore, the actual value of the potential energy barrier for the zirconia sol must be larger than $20\ kT$. This interpretation justifies the observed data shown in Figs. 3 and 4.

The potential energy of heterointeraction between the boehmite–silica composite particle ($a_1 = 100$ nm) and zirconia particle ($a_2 = 25$ nm) for $\psi_{01} = \psi_{02} \approx \zeta = +$ 40 mV (pH 3.5) under various conditions of ionic strength (thus, $\kappa$) was calculated and is displayed in Fig. 6. The curve (1) was calculated under the condition of $10^{-3.5}$ M for the bulk concentration of electrolyte (i.e., $\kappa = 5.85 \times 10^5$ cm$^{-1}$). This approximately corresponds to a dilute sol at a pH of 3.5 without any external addition of inert electrolyte. As is shown in Fig. 6, the potential energy barrier at a pH of 3.5 (curve (1)) is approximately $30\ kT$ with the absence of a shallow potential well. Therefore, one would expect that the boehmite–silica–zirconia mixed sol at a pH of 3.5 is kinetically stable and exhibits Newtonian behaviour before the compression of EDL. This prediction accords with the rheological behaviour of the mixed sol, as is shown in curve (3) of Fig. 3. Although the height and the thickness of the potential energy barrier decrease significantly with increasing ionic strength, the existence of a shallow potential well (the secondary minimum) is not evident over a wide range of ionic strength. Thus, this calculated result does not agree with the observed rheological behaviour at a higher ionic strength (for $M > 5 \times 10^{-3}$ M; curve (4) of Fig. 3).

It was shown that the rheological behaviour of the mixed ternary sol (Fig. 3) undergoes a transition from Newtonian to pseudoplastic after the compression of EDL by the addition of the inert electrolyte, while maintaining low viscosity values. This clearly indicates that the mixed ternary sol forms weakly coagulated units in a shallow potential energy well after the compression of EDL at a pH of 3.5. If the boehmite–silica composite particle forms a coagulated unit with a zirconia particle after the EDL compression, the effective radius of a particle will increase. As is

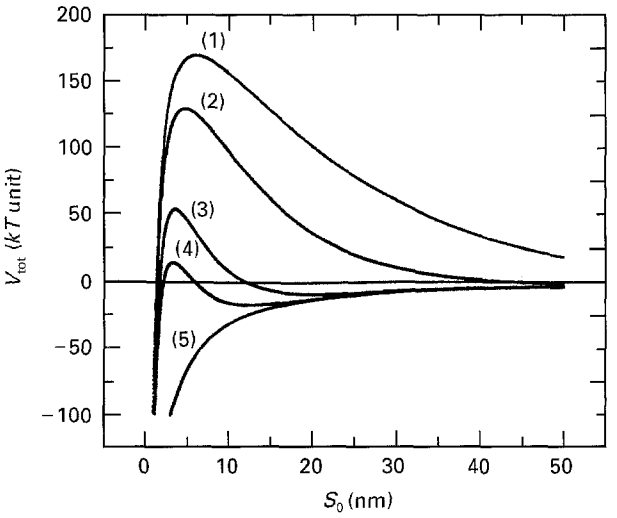


*Figure 7* Potential energy of homointeraction between boehmite–silica–zirconia coagulated units ($a = 250$ nm) for a $\Psi_0$ of + 40 mV under the same conditions of ionic strength as that used in Fig. 6. The numbering in this graph therefore corresponds to that used in Fig. 6.

shown in Fig. 6, the calculated potential energy of interaction for an ionic strength greater than $5 \times 10^{-3}$ M is less than 10 $kT$, supporting the possibility of this coagulation.

Assuming that the boehmite–silica composite particles undergo a heterointeraction with the zirconia particles, forming weakly coagulated units with an effective radius of 250 nm, one can estimate the potential energy of homointeraction between these coagulated units under various conditions of ionic strength. As is shown in Fig. 7, the potential energy of interaction for ionic molarity values between $5 \times 10^{-3}$ $-1.0 \times 10^{-2}$ M exhibits a shallow potential well (secondary minimum), while maintaining a sufficiently large potential energy barrier. Therefore, the calculated result indicates that, after the compression of EDL, the boehmite–silica–zirconia mixed sol at a pH of 3.5 ($\zeta = 40$ mV) undergoes a rheological transition from a kinetically stable state (Newtonian) to a weakly coagulated state in a shallow potential well (pseudoplastic). This justifies our processing scheme on the mixed sol processing and explains the observed rheological data.

## 3.3. Phase-formation characteristics

Fig. 8 presents X-ray diffraction patterns of the unseeded boehmite–silica–zirconia composite pellets heat-treated at various temperatures for 1 h (heating rate, 5 °C per min). Similarly, XRD patterns of the 3 wt % $\alpha$-$Al_2O_3$ seeded specimens heat-treated at various temperatures are shown in Fig. 9. For both specimens, monoclinic $ZrO_2$ begins to transform to tetragonal $ZrO_2$ below 1200 °C, reflecting the thermodynamic stability of the tetragonal phase above ~1150 °C.

Regardless of the $\alpha$-$Al_2O_3$ seeding, the formation of zircon was not observed (Figs. 8 and 9). The observed suppression of zircon formation can be attributed to the presence of alumina. It is known that alumina

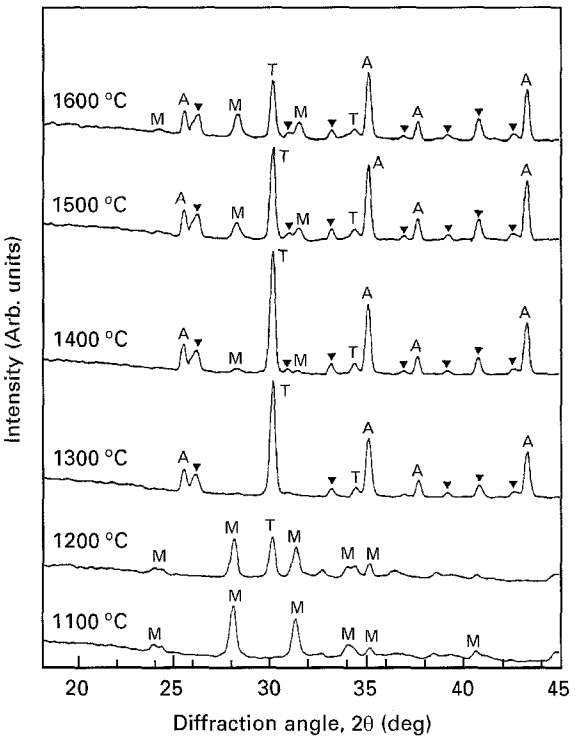


*Figure 8* XRD patterns of the unseeded boehmite–silica–zirconia composite pellets heat-treated at various temperatures for 1 h (A: $\alpha$-$Al_2O_3$, ▼: mullite, T: t-$ZrO_2$, M: m-$ZrO_2$).

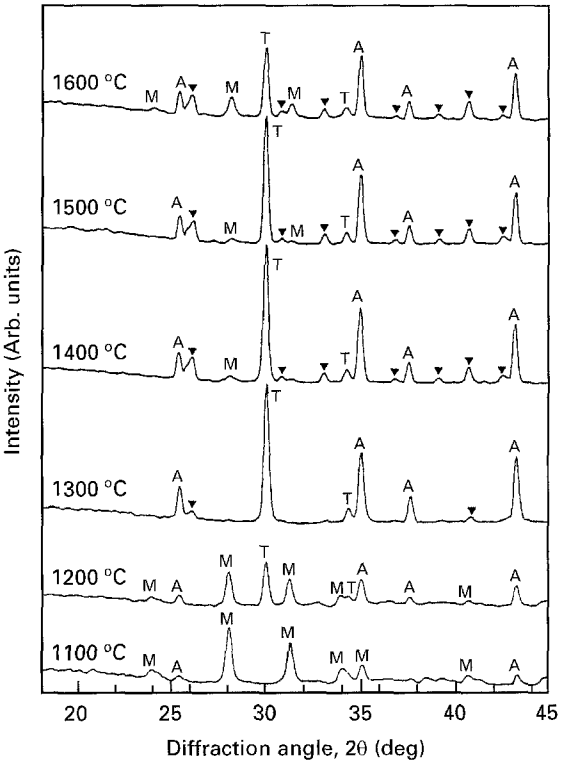


*Figure 9* XRD patterns of the 3 wt % $\alpha$-$Al_2O_3$ seeded boehmite–silica–zirconia composite pellets heat-treated at various temperatures for 1 h (A: $\alpha$-$Al_2O_3$, ▼: mullite, T: t-$ZrO_2$, M: m-$ZrO_2$).

reacts with zircon above 1400 °C, forming mullite and $ZrO_2$ by the following reaction [28, 29] :

$$3Al_2O_3 + 2ZrSiO_4 \rightarrow 3Al_2O_3 \cdot 2SiO_2 + 2ZrO_2 \quad (7)$$

Therefore, the presence of alumina expedites the formation of mullite and suppresses the formation of detrimental zircon.

As shown in Fig. 8, neither $\alpha$-$Al_2O_3$ nor mullite in the unseeded specimen crystallizes until the temperature reaches 1300 °C. On the other hand, the XRD patterns of the seeded specimen (Fig. 9) indicate that the intensity of XRD peaks associated with $\alpha$-$Al_2O_3$ increases gradually (1100–1300 °C) with increasing temperature below 1300 °C. A comparison of the results of Fig. 8 with those of Fig. 9 further indicates that the relative fraction of mullite at 1300 °C is smaller in the $\alpha$-$Al_2O_3$ seeded specimen than in the unseeded specimen. Therefore, one can tentatively conclude that the $\alpha$-$Al_2O_3$ seeding facilitates the formation of $\alpha$-$Al_2O_3$ but suppresses the growth of the orthorhombic mullite phase.

The validity of the above conclusion was carefully examined by estimating the relative peak intensities of $\alpha$-$Al_2O_3$ (corundum) and mullite with respect to a certain standard peak. Since the total content of zirconia remains constant, one can take the total intensity for zirconia ($I_{tot}$) as an internal standard. According to the study done by Garvie and Nicholson [20], $I_{tot}$ can be written as: $I_{tot} = I_m(1\,1\,1) + I_m(1\,1\,\bar{1}) + I_t(1\,1\,1)$, where $I_m(hkl)$ and $I_t(hkl)$ are the integral intensities of the $(hkl)$ peaks of the monoclinic and tetragonal phases, respectively. Since the cubic phase was absent in the composite specimens, no peak intensity contribution from the cubic phase was included in the estimate of $I_{tot}$.

Fig. 10 and 11 show the relative XRD peak intensities of the (1 1 3) plane of $\alpha$-$Al_2O_3$ ($2\theta = 43.36°$) and the (2 1 0) plane of mullite ($2\theta = 26.27°$) plotted as a function of temperature. The data shown in Fig. 10 were taken from the specimens heat-treated at a given temperature for 1 h. On the other hand, the relative peak intensities presented in Fig. 11 were taken from the specimens heated to a desired temperature and cooled immediately without a holding time. As indicated in the figures, the relative fractions of both the

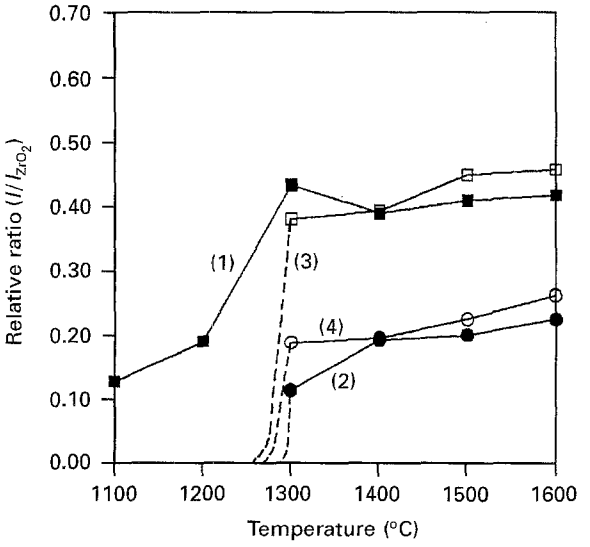


*Figure 10* Relative XRD peak intensities of (1 1 3) plane of $\alpha$-$Al_2O_3$ and (2 1 0) plane of mullite plotted as a function of temperature. The total intensity for zirconia was taken as an internal standard. The specimens were heat-treated at a given temperature for 1 h. The plots are for (1) Seeded, $\alpha Al_2O_3$ (1 1 3), (2) Seeded mullite (2 1 0), (3) Unseeded, $\alpha$-$Al_2O_3$ (1 1 3) and (4) Unseeded, mullite (2 1 0).

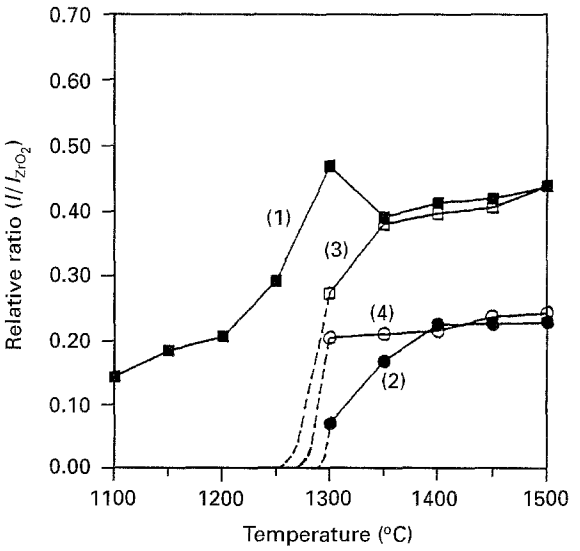


*Figure 11* Relative XRD peak intensities of (1 1 3) plane of $\alpha$-$Al_2O_3$ and (2 1 0) plane of mullite plotted as a function of temperature. The total intensity for zirconia was taken as an internal standard. The specimens were heated to a desired temperature and cooled immediately without holding. The plots are: (1) Seeded $\alpha Al_2O_3$ (1 1 3), (2) Seeded mullite (2 1 0), (3) Unseeded $\alpha Al_2O_3$ (1 1 3) and (4) Unseeded, mullite (2 1 0).

$\alpha$-$Al_2O_3$ and the mullite in the unseeded specimens increased rapidly at 1300 °C. On the other hand, the peak intensity corresponding to $\alpha$-$Al_2O_3$ starts to increase at a temperature (~1100 °C) well below the 1300 °C in the seeded specimen (curve 1 in Figs. 10 and 11), while the formation of mullite is retarded by the $\alpha$-$Al_2O_3$ seeding (curve 2). These effects are more pronounced in the specimens cooled immediately after reaching a desired temperature (Fig. 11). The observed decrease in the relative fraction of $\alpha$-$Al_2O_3$ in the seeded specimen between 1300–1350 °C is directly related to the increase in the intensity of the orthorhombic mullite phase in this temperature range and, thus, can be attributed to the formation of mullite by the reaction of $\alpha$-$Al_2O_3$ with $SiO_2$.

As is shown in Figs. 10 and 11, the two most outstanding effects of $\alpha$-$Al_2O_3$ seeding on the phase-formation characteristics of an AMZ composite are (i) the selective (enhanced) formation of corundum phase between 1100–1300 °C (i.e., lowering in the onset of crystallization to $\alpha$-$Al_2O_3$) and (ii) the retarded formation of mullite. The enhanced formation of $\alpha$-$Al_2O_3$ reflects an epitaxial effect caused by the submicrometer-sized $\alpha$-$Al_2O_3$ seeds. As mentioned previously, the enhanced formation of corundum phase in the presence of seeds is accompanied by the retardation in the formation of mullite (curve 2 in Figs. 10 and 11). The activation free energy for the reaction of transitional aluminas (such as $\gamma$ and $\theta$-polymorphs) with silica must be less than that for the reaction between $\alpha$-$Al_2O_3$ and silica since transitional aluminas are thermodynamically less stable than corundum. Therefore, in the unseeded specimens, mullite is expected to be formed directly from the matrix containing transitional aluminas and silica before unstable alumina polymorph(s) completely transform to the stable corundum phase (curves 3 and 4).

In the seeded specimens, however, the epitaxial effect of the $\alpha$-$Al_2O_3$ seeds preferentially induces the formation of the corundum phase before mullite forms. Thus, the formation of mullite in the seeded specimen is mainly caused by the reaction between stable corundum and silica, which requires a larger activation energy, thus a higher reaction temperature. This explains the observed retardation in the formation of mullite in the presence of $\alpha$-$Al_2O_3$ seeds. The observed temporary decrease in the intensity of the (1 1 3) $\alpha$-$Al_2O_3$ peak during the formation of mullite (1300–1350 °C) in the seeded specimen clearly supports this conclusion.

Examination of the XRD patterns shown in Figs. 8 and 9 suggests that the fraction of tetragonal $ZrO_2$ increases rapidly with increasing temperature and then decreases above a certain critical temperature (~1300 °C). In order to examine this observation more quantitatively, we have estimated the relative phase fractions of the $ZrO_2$ polymorphs using the method outlined by Garvie and Nicholson [20], and these are shown in Fig. 12. It is known [30, 31] that the fraction of tetragonal phase sustained near room temperature after sintering increases with increasing the elastic modulus of the constraining matrix and with decreasing the size of the $ZrO_2$ particles (surface effects). Therefore, the observed decrease in the fraction of tetragonal phase above 1300 °C indicates the growth of zirconia particles with increasing sintering temperature.

As is shown in Fig. 12, the effect of the $\alpha$-$Al_2O_3$ seeding (3 wt %) on the extent of tetragonal zirconia fraction is evident in specimens sintered above 1400 °C. The stabilization of the tetragonal phase in the presence of $\alpha$-$Al_2O_3$ seeds is presumably due to the increase in the sintered density of composite specimens in the presence of seeds. It was observed that, for a sintering temperature above 1400 °C, the $\alpha$-$Al_2O_3$ seeding significantly enhanced the densification of the

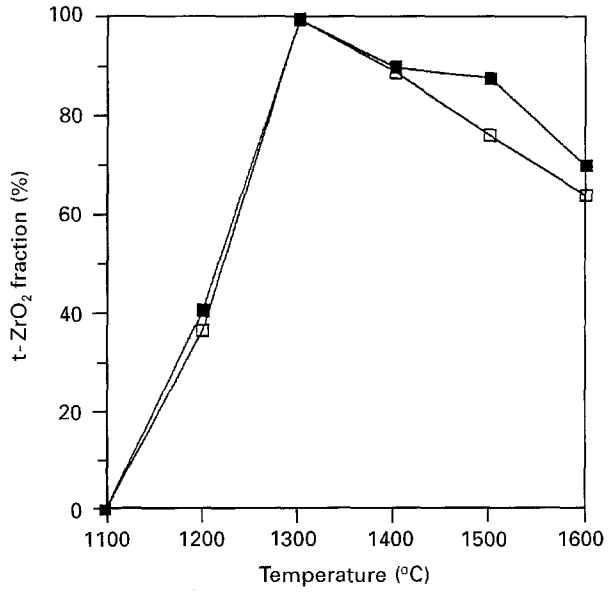


*Figure 12* Fraction of tetragonal $ZrO_2$ as a function of sintering temperature. All the specimens were sintered at a given temperature for 1 h. The data was recorded for (■) Seeded and (□) Unseeded specimens.

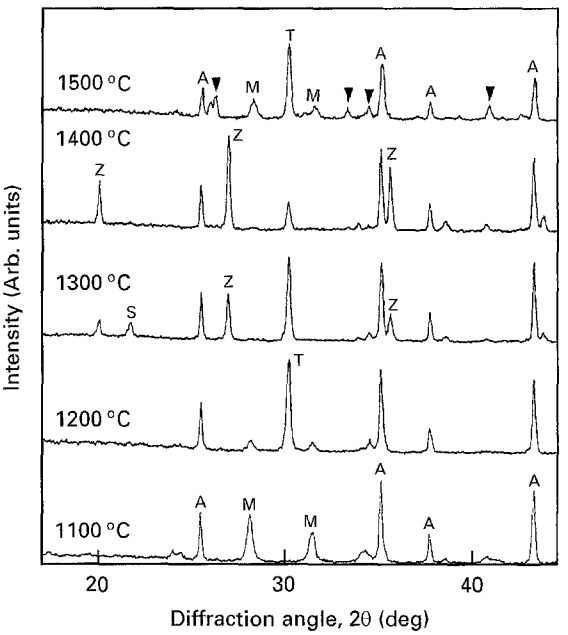


*Figure 13* XRD patterns of the $\alpha$-$Al_2O_3$–silica–zirconia composite pellets heat-treated at various temperatures for 1 h (A: $\alpha$-$Al_2O_3$, ▼: mullite, T: t-$ZrO_2$, M: m-$ZrO_2$, Z: zircon, S; cristobalite).

AMZ composites [17]. The presence of pores after sintering will relieve the stress induced in the matrix and thus decrease the elastic strain energy. Therefore, one can conclude that, for a given sintering temperature or average particle size of zirconia, the fraction of tetragonal phase increases as the sintered density of the matrix increases.

The effects of the nature of the aluminium-containing precursor on the phase-formation characteristics were examined using $\alpha$-$Al_2O_3$, instead of boehmite, as a starting material. Fig. 13 shows XRD patterns of the $\alpha$-$Al_2O_3$–silica–zirconia composite pellets heat-treated at various temperatures for 1 h (heating rate, 5 °C per min). As indicated in the figure, both cristobalite and zircon rapidly form at ~1300 °C. However, the peak associated with cristobalite disappears at 1400 °C, while the relative peak intensity associated with zircon increases significantly as the temperature increases from 1300 °C to 1400 °C. Therefore, the disappearance of cristobalite is caused by the reaction of $SiO_2$ with $ZrO_2$, forming zircon in this temperature range. As the temperature increases further, this zircon reacts with alumina to form mullite and zirconia (Equation 7). The appearance of the peaks associated with mullite at 1500 °C further supports this conclusion.

The observed phase-formation characteristics can be more comprehensively understood by considering the following three relevant solid-state reactions:

$$3Al_2O_3 + 2SiO_2 \text{ (amorphous)} \rightarrow 3Al_2O_3{\cdot}2SiO_2 \quad (8)$$

$$SiO_2 \text{ (amorphous)} + ZrO_2 \rightarrow ZrSiO_4 \quad (9)$$

$$SiO_2 \text{ (amorphous)} \rightarrow SiO_2\text{(cristobalite)} \quad (10)$$

For a composite system prepared with a boehmite precursor, the formation of thermodynamically stable mullite by Equation 8 is the dominant process near

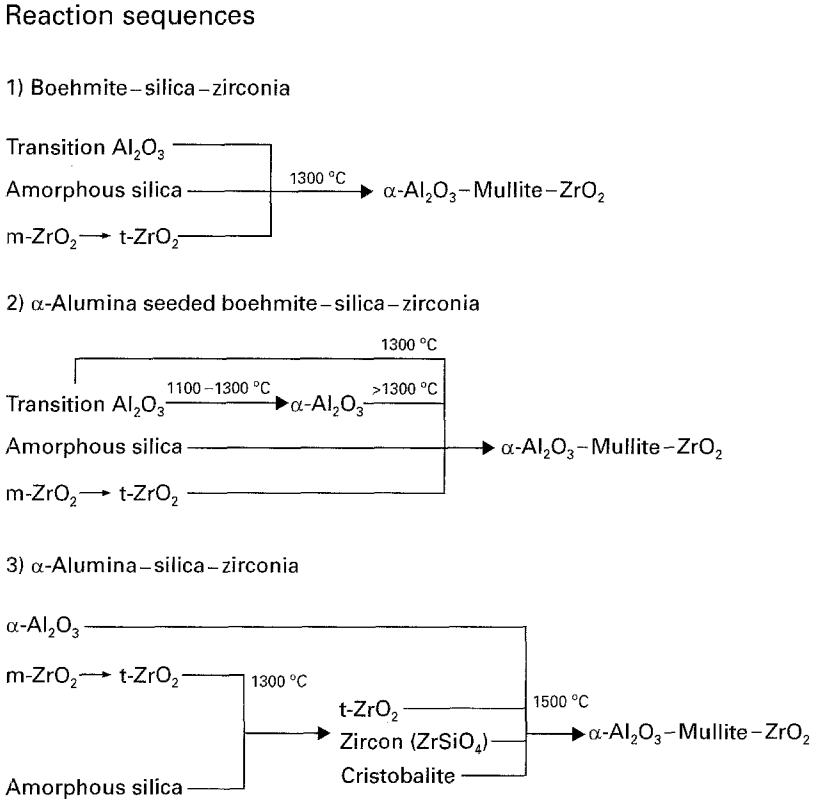


*Figure 14* Mechanisms of phase evolution occurring in the three different types of precursors for alumina–mullite–zirconia composites.

1300 °C (Figs. 10 and 11). In consequence of this, the formation of zircon (Equation 9) and cristobalite (Equation 10) is suppressed. On the other hand, the formation of mullite by Equation 8 is significantly delayed in the $\alpha\text{-}Al_2O_3$–silica–zirconia composite precursor because thermodynamically stable $\alpha\text{-}Al_2O_3$ rather than unstable transitional alumina participates in the formation of mullite. Therefore, the formation of zircon and cristobalite represented by Equations 9 and 10 is facilitated in the $\alpha\text{-}Al_2O_3$–silica–zirconia composite precursor. Therefore, the formation of zircon or cristobalite is directly associated with the delayed formation of mullite in the absence of transitional aluminas and is mainly caused by a kinetic factor. Based on all the observations discussed so far, we were able to delineate the mechanisms of phase evolution occurring in the three different types of precursor systems. These are summarized in Fig. 14.

## 4. Conclusions

A new colloidal processing scheme for fabricating a boehmite–silica–zirconia precursor powder was proposed and tested. The effects of $\alpha\text{-}Al_2O_3$ seeding on the phase-formation characteristics of the precursor systems were then systematically examined. The following conclusions were drawn.

1. A boehmite–silica–zirconia precursor powder with a uniform spatial distribution of constitutive phases was prepared from the corresponding ternary sol by rapidly compressing the electrical double layer (EDL) without altering the magnitude of the surface potential at a pH of 3.5.

2. The rheological data indicated that the boehmite–silica–zirconia ternary sol underwent a transition from Newtonian to pseudoplastic behaviour after the compression of EDL at a pH of 3.5 by the addition of an inert electrolyte, while maintaining low viscosity values.

3. The calculated potential energy of interaction further indicated that the mixed ternary sol formed weakly coagulated units in a shallow potential energy minimum after the compression of EDL at a pH of 3.5.

4. The two most outstanding effects of $\alpha\text{-}Al_2O_3$ seeding on the phase-formation characteristics of alumina–mullite–zirconia composite are (i) the enhanced formation of a corundum ($\alpha\text{-}Al_2O_3$) phase between 1100–1300 °C, and (ii) the retarded formation of mullite. These observations were attributed to an epitaxial effect of $\alpha\text{-}Al_2O_3$ seeds which preferentially induced the formation of the corundum phase before mullite formed in the matrix.

5. The $\alpha\text{-}Al_2O_3$ seeding also increased the fraction of tetragonal zirconia in the alumina–mullite–zirconia composites sintered above 1400 °C.

## References


1. "Advances in Ceramics, Vol. 12, Science and Technology of Zirconia II," edited by N. Claussen, M. Rühle, and A. H. Heuer (American Ceramic Society, Columbus, OH, 1984).
2. N. CLAUSSEN, *J. Amer. Ceram. Soc.* **59** (1976) 49.
3. M. RÜHLE, N. CLAUSSEN and A. H. HEUER, *Ibid.* **69** (1986) 195.
4. D. L. PORTER, A. G. EVANS and A. H. HEUER, *Acta Metall.* **27** (1979) 1649.
5. A. G. EVANS and A. H. HEUER, *J. Amer. Ceram. Soc.* **63** (1980) 241.
6. A. G. EVANS and K. T. FABER, *Ibid.* **67** (1984) 255.
7. K. T. FABER, *Ceram. Eng. & Sci. Proc.* **5–6** (1984) 408.
8. F. F. LANGE, *J. Mater. Sci.* **18** (1983) 255.
9. N. CLAUSSEN, *Mater. Sci. Eng.* **71** (1985) 23.

10. P. A. LESSING, R. S. GORDON and K. S. MAZDIYASNI, *J. Amer. Ceram. Soc.* **58** (1975) 149.
11. A. P. HYNES and R. H. DOREMUS, *Ibid.* **74** (1991) 2469.
12. G. ORANGE, G. FANTOZZI, F. CAMBIER, C. LEBLUD, M. R. ANSEAU and A. LERICHE, *J. Mater. Sci.* **20** (1985) 2533.
13. C. BAUDIN, F. CAMBIER and L. DELAEY, *Ibid.* **21** (1986) 4024.
14. *Idem, ibid.* **22** (1987) 4398.
15. M. KUMAGAI and G. L. MESSING, *J. Amer. Ceram. Soc.* **67** (1984) C230.
16. R. A. SHELLEMAN, G. L. MESSING and M. KUMAGAI, *J. Non-cryst. Solids.* **82** (1986) 277.
17. H. M. JANG, S. M. CHO, and K. T. KIM, *J. Mater. Sci.* **31** (1996), in press.
18. B. C. LIM and H. M. JANG, *J. Amer. Ceram. Soc.* **76** (1993) 1482.
19. P. H. WIERSEMA, A. L. LOEB and J. Th. G. OVERBEEK, *J. Colloid Interface Sci.* **22** (1966) 78.
20. R. C. GARVIE and P. S. NICHOLSON, *J. Amer. Ceram. Soc.* **55** (1972) 303.
21. T. KIMURA, Y. KANEKO and T. YAMAGUCHI, *Ibid.* **74** (1991) 625.
22. H. M. JANG, J. H. MOON and C. W. JANG, *Ibid.* **76** (1993) 3369.
23. H. M. JANG, in "Chemical Processing of Ceramics", edited by B. I. Lee and E. J. A. Pope (Marcel Dekker, Inc., New York, 1994) Ch. 7.
24. J. Th. G. OVERBEEK, *J. Colloid Interface Sci.* **58** (1977) 431.
25. *Idem*, in "Colloid Science", edited by H. R. Kruyt (Elsevier, Amsterdam, 1952) p. 245.
26. S. USUI and S. HACHISU, in "Electrical Phenomena at Interfaces", edited by A. Kitahara and A. Watanabe (Marcel Dekker, Inc., New York, 1984) Ch. 3.
27. A. BLEIER and C. G. WESTMORELAND, *J. Amer. Ceram. Soc.* **74** (1991) 3100.
28. E. DI. LUPO, E. GILBART, T. G. CARRUTHERS and R. J. BROOK, *J. Mater. Sci.* **14** (1979) 705.
29. P. DESCAMPS, S. SAKAGUCHI, M. POORTEMAN and F. CAMBIER, *J. Amer. Ceram. Soc.* **74** (1991) 2476.
30. F. F. LANGE and D. J. GREEN, in "Advances in Ceramics, Vol. 3, Science and Technology of Zirconia", edited by A. H. Heuer and L. W. Hobbs (American Ceramic Society, Columbus, OH, 1981) p. 217.
31. F. F. LANGE, *J. Mater. Sci.* **17** (1982) 225.

*Received 2 October 1995*
*and accepted 18 March 1996*